Microstructure and flexural strength of hafnium diboride via flash and conventional spark plasma sintering

D. Demirskyi (a,b)†, T.S. Suzuki (b), S. Grasso (c), and O. Vasylkiv (b)†.

(a) WPI-Advanced Institute for Materials Research (WPI-AIMR), Tohoku University, 2-1-1 Katahira, Aoba-ku, Sendai, 980-8577 Japan

(b) National Institute for Materials Science, 1-2-1 Sengen, Tsukuba, Ibaraki 305-0047, Japan

(c) Key Laboratory of Advanced Technologies of Materials, Ministry of Education, School of Materials Science and Engineering, Southwest Jiaotong University, Chengdu 610031, China

Abstract

Microstructure evolution in bulk hafnium diboride ceramics prepared by spark plasma sintering in flash regime was compared with conventional spark plasma sintering. The conventional and flash spark plasma sintering resulted in ceramics with a high relative density exceeding 96 % of their theoretical density. A remarkably fine grain size distribution was noticed for the specimen prepared in the flash regime. This atypical microstructure evolution provides a possible insight into the mechanism of flash sintering for conductive bulks. The room temperature flexural strength of the hafnium diboride processed by flash SPS was 650 MPa which is 140 MPa higher than the sample produced by conventional SPS.

Keywords: hafnium diboride; flash sintering; flexural strength; high temperature materials.

1. Introduction

Due to the high melting point and low diffusivity, the consolidation of HfB_2 requires the application of pressure [1–3], or the combination of pressure and a pulsed electrical current [4–6] with temperatures on the order of 2000 °C. Studies of the presureless sintering of bulk

† Authors to whom correspondence should be addressed, Dmytro Demirskyi, demirskyi.dmytro.e2@tohoku.ac.jp /phone +81(0)70-2010-6281/ and Oleg Vasylkiv, oleg.vasylkiv@nims.go.jp /phone +81(0)80-4144-4747/

diborides suggested that a vapor controlled mechanisms is dominant above 2000 °C, which leads to significant particle coarsening without any significant gain in density. Thus pressureless sintering of HfB_2 leads to the coarse grains of 15–22 μm [7].

Furthermore, the presence of surface oxides, such as B_2O_3 and HfO_2, inhibits densification [1,3,7,8]. Thus a promising approach for overcoming these obstacles is to use field assisted sintering techniques which allows: i) high-heating rates to minimize grain coarsening during heating and ii) electrochemical reduction/sublimation of the surface oxides.

From this point of view, a recent modification of the widely used spark-plasma sintering (SPS) method, flash SPS (FSPS), offers an opportunity to utilize heating rates higher than 1000 °C/min. Several ceramics, including SiC, B_4C, and ZrB_2 with diameters up to 60 mm have been consolidated by the FSPS with a discharge time below one minute [9–12]. In this respect, the consolidation of metal-like conductive diborides offers a genuine opportunity for obtaining bulk ceramics, which are hard to consolidate by other methods [11].

For zirconium diboride [9], in particular, it was observed that consolidation during FSPS takes place within ~35 s, and such a short time might not be sufficient to complete the chemical reactions between the free carbon and oxygen-rich layer. The use of the extremely high heating rates of FSPS exceeding 10^4/min might allow near instantaneous full densification of these materials. Apart from this, the very limited time exposure at high temperature might preserve the fine microstructure of the starting powders [11]. Because using the versatility of the FSPS process, large (i.e., ≥ Ø60 mm) bulk diboride ceramics can be consolidated using commercial powders. At present, the relationship between the processing times and properties is still not clear.

The objectives of this study are to obtain dense hafnium diboride ceramics using commercially available powders by FSPS and to gain insight into the consolidation details. In this study, dense HfB_2 monoliths were prepared by the FSPS method at 2000 °C and a 30-

second dwell using the as-received raw powder. The effect of the pre-consolidation conditions, and consolidation method (i.e., flash vs conventional SPS (CSPS)), on the microstructure development was investigated. Furthermore, the flexural strength of thus prepared bulks at ambient temperature and at 1600 °C was tested and analyzed.

2. Experimental

Commercially available HfB_2 (Grade O, Lot # T302510) with an average powder particle size between 1 and 3 μm (Japan New Metals Co. Ltd., Osaka, Japan) was used as the starting material. In this study, the initial HfB_2 powder was found to contain 1.1 to 1.6 wt% of oxygen. Other possible impurities, such as C (0.35 wt%) and N (up to 0.4 wt%) were within the specification provided by the manufacturer (O 0.8 wt.%, C 0.3 wt% and N 0.3 wt%). The total nitrogen, oxygen and carbon contents of the powders were measured again as these might have been affected by the storage conditions. The analyses were done using an ON-900 and CS-800 (Eltra GmbH, Haan, Germany).

The as-received powders were subjected to homogenization in alcohol, followed by drying at about 100 °C. The resultant powders were screened through 60 and 400 mesh screens. The homogenized powder mixture was loaded into a graphite die with an inner diameter of 30 mm and subjected to the SPS. The outer surface of the die was wrapped in 5-mm-thick graphite felt to homogenize the temperature distribution and reduce heat loss by radiation. The mold system containing the powder mixture was placed in an SPS furnace (‘Dr. Sinter’, SPS 1050, Sumitomo, Japan) [12,13]. A two-step consolidation process was used to produce the FSPS and CSPS specimens [9,13]. First, specimens with a diameter of 30 mm and heights of 5–6 mm were prepared by the preliminary SPS consolidation at 1600 °C. The samples were heated under vacuum to 1600 °C at 100 °C/min under the axial pressure of 60 MPa.

After a 20 min dwell at this intermediate step, samples for the FSPS were cooled to room temperature at the rate of 100 °C/min.

After cooling, the specimens were removed from the graphite die and subjected to a mold-free [9,10] FSPS consolidation. This step consisted of wrapping the pre-consolidated HfB_2 specimens with additional graphite foils and placed in a setup described in ref [13]. The Sumitomo unit was operated in the current control mode, thus a current limit of 3000 A was selected based on previous FSPS runs to reach the stationary temperature of 2000 °C.

The temperature during the FSPS experiments was determined by a side pyrometer focused on the side of the graphite felt using an emissivity of 0.90. Because the graphite felt is a thermal insulator, a tolerance for the accuracy of the temperature measurement was considered as ±50 °C. It was estimated that the sample temperature was at least 100 °C hotter than the probed one (*see section 3.1 on temperatures calibration)*.

In the FSPS experiments, a constant uniaxial pressure of 20 MPa was applied. The apparatus was operated in the constant current control mode, thus preliminary studies allowed us to tune the voltage of the FSPS runs to approximately 6 V (**Fig. 1 (e)**). The power was switched off after the selected discharge time, and specimens were allowed to cool to room temperature under unchanged pressure conditions. The FSPS experiments were performed in argon gas at the flow rate of 2 L/min.

For reference, the samples were also sintered using a CSPS configuration. For these studies, SPS was continued after a preliminary consolidation step at 1600 °C. Thus, after the 20-min dwell at 1600 °C in a vacuum, the SPS chamber was backfilled with argon, and the pre-consolidated HfB_2 specimens were heated up to 2000 °C at the rate of 200 °C/min and then held for 5 min. The pressure of 60 MPa was maintained during the consolidation and cooling stages, as the application of lower pressures did not result in dense materials. Each specimen

was gradually cooled to 600 °C at the rate of 100 °C/min, then naturally to room temperature in the furnace. Argon gas at the flow rate of 2 L/min was used.

The sintered specimens were ground using diamond disks with a particle size of up to 0.5 µm. The density of the samples was then measured by the Archimedes method using ethanol as the medium in accordance with ASTM B 963–08.

The three-point flexural strength was determined according Japanese Standard JIS R160 using rectangular bars (2×2×20 mm) cut from the specimens with a diameter of 30 mm using an electric discharge machining. Their lateral surfaces were ground and polished using diamond pastes. The flexural strength tests were conducted at room temperature and at 1600 °C in argon using a Shimadzu AG-X plus system (Shimadzu, Japan) [14]. The span of 16 mm and loading speed of 0.5 mm/min were used. Ten bars were tested for each specimen at room temperature, and four specimens at 1600 °C. In addition, a single specimen was tested at 600 °C and 1200 °C in order to understand the temperature dependence of the flexural strength of the FSPSed specimen.

Microstructural observations and analyses were carried out on the fracture surfaces using a scanning electron microscope (SEM, SU 8000 cold-emission FE-SEM Hitachi). Observations were made on the fractured surfaces after the flexural tests.

3. Results and discussion

In general, the *flash processes* are considered to have an electric discharge time of minute long [11], but application of pressure during the FSPS and its rapid nature often [12] does not allow producing a large (Ø>20 mm) crack-free specimen. The main reason for this cracking during cooling is that the pressing punches are cooler than the specimen's surface, thus after power is switched off, a temperature difference between the punches and specimen causes the cracks. Thus an additional dwell time was essential for producing crack-free specimens.

Mind, that the shrinkage curve in **Fig. 1 (e)** for the specimen #66F (here and afterwards the numbers denote the internal numerical system related to the SEM & strength measurements) serves as a direct indicator that the initial 60-sec long discharge results in an essentially fully dense specimen, but in order to minimize cracking during cooling, an additional 30 sec dwell was used.

3.1 Temperature gradient during FSPS studies

Debate over the temperature probing during the FSPS in particular, and for SPS, in general, is one of the current key problems for researchers. Few solutions have been proposed, such as probing the temperature from the top rather than from the side [9–11], but it is agreed that regardless of the temperature measurement method (i.e., by pyrometer or thermocouple) there is room for localized overheating during the spark plasma sintering. In the present study, the question for accuracy of the temperature measurement was addressed by preliminary FSPS runs using approximately 1-mm thick specimens. HfB_2 has an eutectic reaction with carbon at approximately 2340 °C [15] or below 2400 °C [16]. These temperatures can be used as a marker for calibration, which is a common procedure when calibrating pyrometers. Thus, there is a possibility for the formation of a ceramic with the quasi-eutectic HfB_2–C structure in the case of the local overheating on the 'graphite felt–specimen' interface. Our previous studies of B_4C–NbB_2 [17] showed that eutectic formation during SPS is accompanied with a rapid shrinkage. Thus, in order to understand the minimum allowed gradient during the FSPS experiments using the Sumitomo unit, we attempted to identify the temperature for the maximum shrinkage rate if the eutectic reaction between HfB_2 and carbon is triggered. The results of these trial experiments are illustrated in **Fig. 2**.

For the specimen #100 presented in **Fig. (2 (a)),** the temperature at which a rapid shrinkage was initiated was evaluated as high as 2220 °C. The SPS was then stopped after this rapid

increase in shrinkage was noticed. The general fracture and analysis of the polished surface suggested that (a) elongation of the HfB_2 grains was quite visible, and (b) the graphite phase percolates in the area between diboride grains. These are most likely to be a consequence of eutectic formation. In this case, the temperature difference between the previously reported temperature and probed in situ during the FSPS using a side pyrometer set-up was approximately 120 °C, which may be considered as a first approximation inaccuracy inherent to the temperature probing.

In addition, **Figure 2** (b) shows that the structure of the trial specimen using a 2000 °C FSPS run is free from elongated grains, but resulted in a crack-free specimen, thus it was suggested that the temperature of 2000 °C should be used for the HfB_2 consolidation. Because of the dimensions of the specimens obtained in the preliminary runs, the mechanical performance cannot be evaluated. Some large sized grains observed in **Fig. 2 (b)** can be viewed as a local overheating caused by contact with the upper punch of the SPS unit. In both presented cases, the current flow during the FSPS consolidation process was from left to right. The majority of grains in the middle of the specimen #88 cross-section was between 10 and 20 microns. Here, one should take into account that the temperature distribution while comparing 1-mm thick and 5-mm thick specimen is expected to be different and may be a good challenge for temperature simulation studies, and thus may lead to different grain sizes. Nevertheless, in order to deal with ‘overheated’ area in the present study, rather thick specimens were prepared for the FSPS runs, and eventually during preparation of the specimens for the flexural tests, this thin surface was polished off. Thus fracture surfaces subjected to the analysis represent the middle section of the FSPSed specimen.

3.2 Effect of SPS processing mode on the microstructure

The fractional density of the hafnium diboride bulks prepared by FSPS and CSPS is (#66F) 97.9% and (#61) 96.9%, respectively. The only crystalline phases were identified as HfB_2 (PDF #38-1398).

Despite the similarity in the fractional density, a clear difference in the grain-size distribution was observed between specimens consolidated using the different methods. The SEM fractographs of the fractured surfaces shown in **Figs. 3** and **4** [2,3,6,18,19] illustrate the difference in the final microstructure.

The FSPSed hafnium diboride possessed a clear bimodal grain size distribution, which is macroscopically similar to that expected for the dual architecture composites [20], thus making it in some sense dual architecture 'monolith'. This type of structure can be considered the initial stage of the grain-growth for some ceramics [21], as large grains occupied roughly 1/5 of the fracture surface. A previous study [22] predicted that the normal grain growth will take place if the grain boundaries are isotropic, and the grain growth rate is linear with the driving force. Hence, the data for the FSPS suggest that a non-linear correlation between the grain growth and the capillary driving force (i.e., curvature between grains) may occur during a dwell at high temperature, i.e., a stage where densification prevails over grain growth is expected at the high-heating rate stage of the 'flash' consolidation process. It is assumed that the final stage of consolidation usually associated with pore closure is not being affected by the FSPS. Thus after the density exceeding 90 % is achieved, a conventional increase in the grain size, (to a lesser extent) and in density will take place. Because the grain growth process is quite sensitive to exposure to high temperatures, a bimodal grain size distribution can be associated with a short made during FSPS (**Fig. 1 (e)**). Without a doubt, an additional 30 seconds of dwell during the FSPS may be sufficient time for the observed grain growth (compare with **Fig. 2 (b)**, but mind different heating rates), but further experiments on this subject are required. At first approximation, **Fig 2 (b)** indicates the possibility of local grain

growth at the upper SPS electrode–graphite felt–specimen interface. This may be attributed to the local *surface* overheating, and regarding specimen #66F, the initial thickness of the green specimen was much higher, and any anomalies observed can be considered to be caused by the local *bulk* overheating and thus associated with the current flow through the specimen.

Alternatively, for TiB_2 [8], the existence of a zone with finer/coarser grains was previously attributed to a strong reducing environment around the specimen created by the graphite crucible during hot-pressing. Because the graphite crucible was used only for the pre-consolidation stage in the case of the FSPS, the structure obtained during the flash stage cannot be fully attributed to the findings in Ref. [8].

Thus in order to understand the *bulk* effects in HfB_2 during the FSPS process, one should take into account that (a) a completely random distribution of 'chains' consisting of coarser grains, and (b) after the flexural test, we see the surface that is perpendicular to the current flow and to the pressure direction. Thus a process of a 'flash'-type consolidation suggested in [23] is also possible. Namely, spark-like impulses that follow the string of conductive particles [24] are expected to be the main source for heating/densification for conductive powder materials. In this situation, a percolating network of large particles might also serve as an additional driving force for densification. It is thought that formation of the bimodal-type structure is mainly due to a short dwell at flash temperature, noting that pores were rarely observed after the FSPS.

Furthermore, as **Fig. 1 (c)** shows, after the preliminary consolidation, some grains had surface markings that resemble that after a surface diffusion or evaporation-based mechanism [21]. A preconsolidation step at 1600 °C did not result in a significant grain growth and densification (density bellow 60 % TD, 1–5 μm). In fact, the relative density of the as-received HfB_2 hot pressed at 2200 °C was only 85.8 % and the densification of HfB_2 by hot pressing started above 1650 °C [3]. This suggests that non-densifying mechanisms, such as vapor-

condensation, were active. This also agrees with findings of of B_2O_3 volatilization [3,7] in this temperature range. Because during the SPS (similar to hot pressing), the graphite mold may also serve as an additional source of C, CO or CO_2 [8, 12], a vapor induced crystal growth observed in preconsolidated specimen, may result in an oxygen decrease, as preliminary results suggest that the oxygen level for bars after the flexural tests was 0.34 wt.%, which is quite helpful in achieving high bulk density diborides [7]. Specifically, in order to be subjected to FSPS, the reconsolidated bulks are required to have a fairly good level of mechanical properties as the flexural strength of 305±25 MPa was measured for the reconsolidated specimen.

In the case of the CSPS runs, during a comparable 1-min dwell run at 2000 °C, the CSPS resulted in a density below 92 %, thus a much longer dwell time was required to achieve a density comparable to that for the FSPS. As result, after 5-min exposure at 2000 °C, the grain size of HfB_2 was 10–18 μm (**Fig. 4**). The majority of the pores was located within the grains, suggesting the domination of grain growth over densification. We also observed the presence of a secondary phase (undetectable by XRD) which is thought to have a nature similar to that previously obverted for TaC [25], i.e., a non-stoichiometric carbide phase.

For the, lower limit of the grain size, i.e., 10 μm, is close to the large grains for the FSPSed specimen. This also serves as an indirect indicator of the local *bulk* overheating [12] and grain growth during the FSPS process. Importantly, an analysis of the densification behavior of HfB_2 in [3] suggests that in order to reach a high density, a dwell of 60 min is required at 1900 °C, which suggests that a complex combination of mass transport processes is expected.

3.3 Analysis of FSPS sintering kinetics using non-isothermal sintering approach

The typical profile presented in **Fig. 1 (e)** was quite common within the specimens obtained in the present study, and one can easily divide it into three areas. For simplicity, these are

clearly indicated in **Fig. 5**, where the output of the Sumitomo unit represents the temperature dependence of shrinkage. Here one can see that the flash sintering during the FSPS is essentially finished by 2000 °C. At this temperature, a change in shrinkage is not observed. At this point, the powder specimen has achieved full density (similar to #88 **Fig. 2 (b)**), but an additional dwell was added to equilibrate the temperature distribution within the relatively thick specimen to avoid cracking.

One can see that, in the high-temperature dwell zone, a slight change in shrinkage was observed, which can be viewed as an activation of the initial stage for the grain growth. Anyhow, the plot of the natural logarithm of the shrinkage rate as a function of the inverse value of the absolute temperature (**Fig. 6**) provides additional information on this subject. First, the flash sintering step is be completed at around 1800 °C, where the shrinkage change becomes insensitive to the temperature observed for the FSPSed specimen of HfB_2. Furthermore, based on an almost linear dependence of the shrinkage in **Fig. 7**, it can be assumed that for the temperature range between 900 °C to 1800 °C, the FSPS process may be controlled by a single mechanism (**Fig. 8**). It is noted that other FSPSed specimens of HfB_2 produced with a similar heating profile without dwell (i.e. #88) also shared a linear dependence of shrinkage up to ~1800 °C.

After the densification is completed, it is assumed that the plateau and the zone with an inverse shrinkage dependence up to 2012 °C is due to the competition between the grain-growth and densification presumably by vapor-controlled mechanisms. This is followed by a rapid increase in shrinkage which is being associated with the uncontrolled temperature increase, when the power for the SPS unit was intentionally turned off.

The activation energy for the densification based on the slope for this zone was estimated in **Figs. 7** and **8**. The apparent activation energy (nQ) based on the unaltered #66F data was 33±4 kJ/mol. Within a close approximation, the activation energy of the densification process

can be evaluated using n equal to 1, 1/2 and 1/3 for the viscous flow, volume or grain-boundary diffusion, respectively [26]. Although the model in [26] was developed for the conventional sintering, in the case of SPS and constant pressing conditions, the shrinkage data can be analyzed using the conventional (pressureless) sintering equations [27].

This yields an activation energy of 66 kJ/mol for the grain boundary diffusion and 99 kJ/mol for the volume diffusion. Nevertheless, because there is an uncertainty that is associated with the temperature measurements performed during the flash sintering experiments in general, and in the case of the FSPS, in particular, we attempted to evaluate the activation energies for the densification taking into account the possible overheating of 100 °C and 300 °C. These results are presented in **Fig. 8** and **Table 1** [28–33]. The nQ of 37 to 45 obtained from **Fig. 8** in the case of the local overheating provides an activation energy of 74 to 90 kJ/mol for the grain-boundary diffusion and 111 to 135 kJ/mol for volume diffusion.

A possible effect of pressure on the densification process during the FSPS can be addressed in further studies. Due to the findings in refs.[27] and [34], it was found that an increase in pressure will affect the consolidation process during the pressure assisted flash sintering. It was summarized in [34] that an applied uniaxial stress during sinter-forging also affects the threshold temperature for the flash sintering. As the stress is increased, the temperature for the onset of flash sintering is reduced. In another study [27], it was reported that application of pressure-assisted and conventional sintering analysis for the spark plasma sintering of zirconia will yield identical activation energies when the process is being controlled by a single mechanism of grain-boundary diffusion.

Based on the data presented in **Table 1**, one should highlight that in the case of the high-pressure hot pressing of HfB_2, the activation energy of 96 kJ/mol was reported [29]. Other data for ZrB_2 and TiB_2 collected by different methods yielded an activation energy higher than 400 kJ/mol. Thus in ref. [32], for TiB_2, it was argued that such a high activation energy

may be associated with diffusion of the metal into the metal diboride lattice (like in [19] for TaB_2), since the activation energies for the diffusion of B into TiB or TiB_2 are reported to be ~190 kJ/mol [33]. Here one should point that heating rate may influence a number of mechanisms simultaneously contributing to densification, but the rule of thumb for SPS is that high heating rate allow one to avoid surface diffusion induced coarsening [35].

Compared with the values estimated from **Fig. 8** with that previously reported for transition metal diborides, one can assume both stages to be controlled by the bulk diffusion of boron in the diboride, which becomes especially clear taking into account possible overheating at the interface between the specimen and the graphite felt.

In general, the situation observed during consolidation at elevated temperatures can be illustrated in **Fig. 9**. The area where the majority of the flash experiments on non-oxide ceramics is located on the left side of **(a)**. It is expected that the activation energy of the coarsening process has the lowest activation energy, while the activation energy for the grain growth via bulk diffusion is the highest one. This is true for the majority of metals and ceramics, but in the latter case, it is possible that anions of the metal and non-metal will have a different activation energy and the preexponential factor [36], similar to the finding listed in **Table 1**.

This implies that even in the case of the dominant consolidation mechanism, the identification process of the main diffusion mechanism and diffusing species can be complicated. Two or more mechanisms usually contribute to consolidation at the same time, which significantly complicates analysis, because it is well known that porous ceramics require higher temperatures than the bulk one. Thus the development of the bimodal structure observed for the FSPSed HfB_2 becomes possible if one reaches temperatures in the window of opportunity identified in **Fig. 9**. In this range even a small (e.g., 1 °C or 100 °C) thermal gradient can cause a local increase in the grain growth rate (**Fig. 9 (b)**), given that a sufficient

driving force is available in the consolidated specimen. Furthermore, the inability to 'freeze' the consolidation immediately at a specified point adds more uncertainty to the subject of the grain growth process.

Thus it can be emphasized that analysis of the shrinkage kinetics for the presented hafnium diboride is a preliminary attempt to understand the consolidation mechanism for the flash spark plasma sintering. We should point out that a radial expansion during FSPS was minimized to 100 μm, while the displacement measured by SPS was in the axial direction (up to 2 mm after cooling, when green specimens were ~ 6mm thick). This may contribute to an error during evaluation of the activation energy using specimens axial shrinkage rate. Other aspects of this process associated with grain growth, or the effect of pressure, electrical field, and the *effect of the heating rate* on the FSPS process are expected to be analyzed in a separate study. In the absence of available experimental data for other diborides via FSPS or CSPS, these aspects remain unanswered.

3.4 Flexural strength performance of bulk hafnium diboride prepared using FSPS and CSPS

At room temperature, the flexural strength of the FSPSed specimen was higher than that produced by CSPS, i.e. 650±45 MPs and 512±35 MPa, respectively. At room temperature, the bimodal structure of HfB_2 resulted in a higher flexure strength and had a difference in the loading–stress curves (see **Fig. 2 (g)** and **Fig 10**), which hints that the finer and coarser grains fracture in multiply stages similar to the matrix-fiber composites [37]. Such a loading curve was observed for 4 out of 10 specimens and their flexural strength was above 640 MPa. In the case when a typical linear fracture was observed, the strength was within 623±31 MPa. A slightly lower value in the case of the CSPS specimen can be explained by the Hall-Petch-like relation (see **Fig. 3 (e)** [2,3,6,18,19]).

A closer examination of the macroscopic fracture surface of the bars (**Fig. 10**) showed that a different distribution of the large-sized grains (highlighted by red color) could explain the strange behavior of the FSPSed specimens during flexure. Specimens with a linear loading–stress curve had a different distribution of the large-sized grains. Specimens with a linear behavior of the loading–stress curves fractured in blocks (highlighted in **Fig. 10 (b)**). During fracture in these specimens **(Fig. 10 (b))** the grains with a size of 10–18 µm were not isolated from each other as for the specimen presented in **(Fig. 2 (a))** or **(Fig 10 (a))**. Thus it is assumed that the work of fracture increases if the large-sized HfB_2 grains participate in the fracture of the material, i.e., the fine-grained HfB_2 'matrix' does not fracture before the large-sized HfB_2 grains contribute to the macroscopic fracture. In both cases, the large-sized grains act as a reinforcement phase and fracture trans-granularly. The high values of the strength for these ceramics are likely caused by the grain refinement (see **Fig. 3 (c)**). Because of the lack of information on the fracture of ceramics with this unusual grain size distribution, and because the flexure bars were prepared from a single specimen, it is possible that the different grain size distribution may represent different stages of the grain growth / densification during FSPS.

Furthermore, it is clear that work to fracture for the FSPSed HfB_2 was slightly higher at room temperature (0.62 vs 0.35 J/m^2, for the FSPS and CSPS, respectively). This implies that hafnium diboride after the FSPS fractures "like a" composite [37], where the large HfB_2 grains serve as a reinforcing phase of the matrix consisting of fine-grained HfB_2 (hence the change in slope can be seen during the flexural test). Alternatively, a high work to fracture is due to thermal stresses induced by the high heating/cooling rates during the FSPS processing. However, in the absence of further experiments with ceramic bulks with bimodal grain size distributions, this question remains unanswered.

After the flexural tests at 1600 °C, the fracture of the FSPSed and CSPS was much smoother than that at room temperature. The appearance of rounded grains (i.e., number of grains with sharp corners decreased substantially) was very noticeable due to the activation of plastic deformation and surface diffusion. In terms of the flexural strength, at 1600 °C, the FSPS and CSPS specimens showed a remarkable difference. With an increase in the temperature, the FSPSed specimens showed a rapid decrease in strength; to 282±19 MPa at 1600 °C, while in the case of the CSPSed specimens, a slight decrease in the flexural strength was observed, i.e. 493±24 MPa.

The FSPS specimen showed a gradual decrease in strength (**Fig. 11**) [2,25,38–41] and behaved in a quasi-plastic manner even at 1200 °C, in contrast, the CSPS specimens showed a slight plasticity at 1600 °C. Hence, the flexure strength difference between specimens at 1600 °C is more likely to be a combination of plastic deformation and grain size. Kalish et al. [2] observed an increase in the flexural strength of HfB_2 from 25 °C to 1000 °C, i.e. 344 MPa to 460 MPa, followed by a rapid decrease at 1400 °C, where a strength below 200 MPa was observed. It was argued that a decrease in strength can be attributed to heterogeneous slip processes and elastic residual stresses.

In this study, even at 1600 °C, some HfB_2 grains for the CSPS specimen fractured in a trans-granular manner. Similar to the observation in [2,40], a number of grains fracturing in a transgranular manner may control the strength. Therefore, because intergranular fracture dominates in the FSPS case at elevated temperatures (presumably because the grain size is much different than that in the CSPS case), this may also be an indirect indication of the strength decrease.

This is in good agreement with the general observation that the large grain ceramics are naturally more resistant to creep than the finer grained ceramics at elevated temperatures. In the present study, an FSPS specimen with a unique microstructure showed some plasticity at

600 °C, and a further increase in temperature thus lead to a gradual strength decrease (see **Fig. 2 (g)**). Other factors that might affect the strength at elevated temperatures are (i) short processing time (compare 1 min vs 5 min for the FSPS and CSPS at 2000 °C, or as high as 60 min. at 1900 °C for hot pressing [3]), and (ii) the relaxation of the internal thermal stresses [42,43] induced by rapid processing of the hafnium diboride during the FSPS. Due to local stress gradient, which is a direct result of the temperature gradient during FSPS, some of the preliminary specimens had macroscopic cracks. This is a crucial factor when scaling up, e.g., from 1 to 5 mm thickness, but an additional short dwell at elevated temperature seems to be a vital step to equilibrate the temperature within a specimen and thus increase the chances of obtaining a crack-free specimen [12]. This allows further optimization of the FSPS process, if the generation of an abnormal structure reported in the present study is not required.

4. Conclusions

In summary, as received, coarse HfB_2 powder, was subjected to pre-densification by SPS and then consolidated to a high density using CSPS and FSPS without sintering aids. Rapid consolidation (total discharge time below 60 s) using FSPS resulted in a bimodal grain size distribution, where large-sized 10-μm grains were evenly distributed in the specimen consisting of 1 to 5 μm grains. A comparable density was achieved by CSPS only after a 5-minute dwell at 2000 °C, but associated with significant grain growth. Such a difference in grain size suggests complex densification mechanisms of the flash-type processes, which may be favorable to the development of unique structures. The flexural strength results confirm that despite ultra-rapid processing, ceramics with a strength of 650 MPa were attained.

Acknowledgments

D.D. was supported by World Premier International Research Center Initiative (WPI), MEXT, Japan. S.G. was supported by Thousand Talents Program of China and Sichuan Province.

References

[1] W.G. Fahrenholtz, G.E. Hilmas, I.G. Talmy, J.A. Zaykoski, Refractory Diborides of Zirconium and Hafnium, J. Am. Ceram. Soc. 90 (2007) 1347–1364.

[2] D. Kalish, E. V. Clougherty, K. Kreder, Strength, fracture mode, and thermal stress resistance of HfB2 and ZrB2, J. Am. Ceram. Soc. **52** (1969) 30–36.

[3] H.J. Brown-Shaklee, W.G. Fahrenholtz, G.E. Hilmas, Densification Behavior and Microstructure Evolution of Hot-Pressed HfB2, J. Am. Ceram. Soc. **94** (2011) 49–58.

[4] D. Sciti, S. Guicciardi, M. Nygren, Densification and mechanical behavior of HfC and HfB2 fabricated by spark plasma sintering, J. Am. Ceram. Soc. **91** (2008) 1433–1440.

[5] S. Venugopal, A. Paul, B. Vaidhyanathan, J.G.P. Binner, A. Heaton, P.M. Brown, Synthesis and spark plasma sintering of sub-micron HfB2: Effect of various carbon sources, J. Eur. Ceram. Soc. **34** (2014) 1471–1479.

[6] E. Zapata-Solvas, D.D. Jayaseelan, H.T.Lin, P. Brown, W.E. Lee, Mechanical properties of ZrB2-and HfB2-based ultra-high temperature ceramics fabricated by spark plasma sintering, J. Eur. Ceram. Soc. **33** (2013) 1373–1386.

[7] J. Zou, G.-J. Zhang, Y.-M. Kan, T. Ohji, Pressureless sintering mechanisms and mechanical properties of hafnium diboride ceramics with pre-sintering heat treatment, Scr. Mater. **62** (2010) 159–162.

[8] S. Baik and P.F. Becher, Effect of oxygen contamination on densification of TiB2, J. Am. Ceram. Soc., **70** (1987) 527–530.

[9] S. Grasso, T. Saunders, H. Porwal, O. Cedillos-Barraza, D. Jayaseelan, W.E. Lee, M. Reece, Flash spark plasma sintering (FSPS) of pure ZrB2, J. Am. Ceram. Soc. **97** (2014) 2405–2408.

[10] S. Grasso, T. Saunders, H. Porwal, B. Milsom, A. Tudball, M. Reece, Flash spark plasma sintering (FSPS) of α and β SiC, J. Am. Ceram. Soc. **99** (2016) 1534–1543.

[11] M. Yu, S. Grasso, R. Mckinnon, T. Saunders, M.J. Reece, Review of flash sintering: materials, mechanisms and modelling, Adv. Appl. Ceram., **116**:1 (2017) 24–60.

[12] D. Demirskyi, O. Vasylkiv, Hot-spots generation, exaggerated grain growth and mechanical performance of silicon carbide bulks consolidated by flash spark plasma sintering, J. Alloys Compd. **691** (2017) 466–473.

[13] O. Vasylkiv, H. Borodianska, Y. Sakka, D. Demirskyi, Flash spark plasma sintering of ultrafine yttria-stabilized zirconia ceramics, Scr. Mater. **121** (2016) 32–36.

[14] D. Demirskyi, O. Vasylkiv, Analysis of high-temperature flexural strength behavior of B4C–TaB2 eutectic composites produced by in situ spark plasma sintering, Mat. Sci. Eng. A. **697** (2017) 71–78.

[15] Kosolapova, T.Ya (ed.) Properties, Preparation and Application of High-Melting Compounds: Reference Book, Metallurgiya, Moscow, 1986 [in Russian].

[16] J. M. Criscione, R. A. Mercuri, E. P. Schram, A. W. Smith and H. F. Volk: High Temperature Protective Coatings for Graphite, ML-TDR-64-173 Part XI (1964).

[17] D. Demirskyi, Y. Sakka, *In Situ* Fabrication of B4C–NbB2 Eutectic Composites by Spark–Plasma Sintering, J. Am. Ceram. Soc., **97** (2014) 2376-2378.

[18] Z. Wang, X. Liu, B. Xu, Z. Wu, Fabrication and properties of HfB2 ceramics based on micron and submicron HfB2 powders synthesized via carbo/borothermal reduction of HfO2 with B4C and carbon, Int. J. of Refract. Metals Hard Mater., **51** (2015) 130–136.

[19] D. Demirskyi, O. Vasylkiv, Consolidation and grain growth of tantalum diboride during spark plasma sintering, Ceram. Int., **42** (2016) 16396–16400.

[20] F. Monteverde, C. Melandri, S. Failla, R.J. Grohsmeyer, G.E. Hilmas, W.G. Fahrenholtz, Escape from the strength-to-toughness paradox: bulk ceramics through dual composite architectures, J. Eur. Ceram. Soc. **38** (2018) 2961–2970.

[21] S.-J.L. Kang, Sintering: Densification, Grain Growth and Microstructure, ElsevierScience Publishers, Oxford, 2005.

[22] C.V. Thompson, H.J. Frost, F. Spaepen, The relative rates of secondary and normal grain growth, Acta Metall. **35** (1987) 887–890.

[23] R Marder, C. Estournes, G. Chevallier, R. Chaim, Numerical model for sparking and plasma formation during spark plasma sintering of ceramic compacts, J. Mater. Sci., **50** (2015) 4636–4645.

[24] R. Holm, Electrical contacts, theory and application, Springer-Verlag, Berlin, 1967.

[25] D. Demirskyi, T. Nishimura, Y. Sakka, O. Vasylkiv, High-strength TiB2–TaC ceramic composites prepared using reactive spark plasma consolidation, Ceram. Int., 42 (2016) 1298–1306.

[26] W.S. Young, I.B. Cutler, Initial Sintering with Constant Rates of Heating, J. Am. Ceram. Soc., **59** (1970) 659–663.

[27] H. Borodianska, D. Demirskyi, Y. Sakka, P. Badika, O.Vasylkiv, Grain boundary diffusion driven spark plasma sintering of nanocrystalline zirconia, Ceram. Int., **38** (2012) 4385–4389.

[28] D. Kalish, E.V.Clougherty, Densification Mechanisms in High-pressure Hot-Pressing of HfB2, J. Am. Ceram. Soc., **52** (1969) 26–30.

[29] J.M. Lonergan, W.G. Fahrenholtz, G.E. Hilmas, Sintering Mechanisms and Kinetics for Reaction Hot-Pressed ZrB2, J. Am. Ceram. Soc., **98** (2015) 2344–2351.

[30] M.A. Kuzenkova, P.S. Kislyi, The Mechanism of Shrinkage of Zirconium Diboride During Sintering, Sov. Powder Metall. Met. Ceram., **5** (1966) 114–121.

[31] M. Ouabdesselam, Z.A. Munir, The sintering of combustion-synthesized titanium diboride, J. Mater. Sci., **22** (1987) 1799–1807.

[32] D. Demirskyi, J. Cheng, D. Agrawal, A. Ragulya, Densification and grain growth during microwave sintering of titanium diboride, Scr. Mater., **69** (2013) 610–613.

[33] H. Schmidt, G. Borchardt, C. Schmalzried, R. Telle, S. Weber, H. Scherrer, Self-diffusion of boron in TiB2, J. Appl. Phys., **93** (2003) 907–911.

[34] Francis, John Stanley Curtis, "A Study on The Phenomena of Flash Sintering with Tetragonal Zirconia" (2013). Mechanical Engineering Graduate Theses & Dissertations. 66. [https://scholar.colorado.edu/mcen_gradetds/66].

[35] Y. Aman, V. Garnier, E. Djurado, Spark Plasma Sintering Kinetics of Pure a-Alumina, J. Am. Ceram. Soc., **94** [9] (2011) 2825–2833.

[36] J.W. Christian, The Theory of Phase Transformation in Metals and Alloys,. Part 1, 2nd edition, Pergamon, Oxford, 1965.

[37] A. Kelly, Strong Solids, 2nd ed., Clarendon Press, Oxford, 1986.

[38] E.W. Neuman, G.E. Hilmas, W.G. Fahrenholtz, Strength of Zirconium Diboride to 2300°C, J. Am. Ceram. Soc. **96** (2013) 47–50.

[39] Neuman, Eric W., "Elevated temperature mechanical properties of zirconium diboride based ceramics" (2014). Doctoral Dissertations. [http://scholarsmine.mst.edu/doctoral_dissertations/2164/].

[40] E.V. Clougherty, D. Kalish, E.T. Peters. Research and Development of Refractory Oxidation Resistant Diborides. Technical Report AFML-TR-68-190, ManLabs Incorporated, Wright Patterson Air Force Base, OH; 1968.

[41] D. Demirskyi, O. Vasylkiv, Flexural strength behavior of a ZrB2–TaB2 composite consolidated by non-reactive spark plasma sintering at 2300 °C, Int. J. Refract. Met. Hard Mater., **66** (2017) 31–35.

[42] D. Demirskyi, I. Solodkyi, T. Nishimura, Y. Sakka, O. Vasylkiv, High-temperature strength and plastic deformation behavior of niobium diboride consolidated by spark plasma sintering, J. Am. Ceram. Soc., **100** (2017) 5295–5305.

[43] J. Watts, G. Hilmas, W.G. Fahrenholtz, D. Brown, B. Clausen, Measurement of thermal residual stresses in ZrB2–SiC composites, J. Eur. Ceram. Soc., **31** (2011) 1811–1820.

Figure captions

Fig. 1. Structure evolution during FSPS of HfB_2 monoliths: (a) original powder, (b)–(d) show a fracture surface of typical 'green' specimen after three-point flexure at room temperature. (e) shows output of Sumitomo unit during FSPS run at 2000±50 °C. Mind that after roughly 50 seconds, the specimen reached a plateau in temperature, where it is thought that the consolidation dwell time starts. The SPS is manually switched off after experiencing a slight increase in temperature (and thus shrinkage), which may be an indirect indicator that the full density of the specimen was reached. Prior to that we experienced only a slight increase in the macroscopic shrinkage after reaching the temperature of ~ 1920 °C. Note that after reaching the peak voltage of 6 V, the voltage slowly decreased, which is an indirect indication of the specimen densification.

Figure 2 Structure of the bulk hafnium diboride specimens after FSPS with maximum temperature of (a) (#100) 2220 °C and (b) (#88) 2000 °C (no dwell in both cases), and moderate heating rate of 800 °C/min was used via manual control of the SPS power (~30% of total power) in order to improve the accuracy of the temperature measurements. Inset in **(a)** shows the polished surface of HfB_2 specimen (left side in the **(a)**). Note that for the specimen presented in (b), some local grain growth can be seen on the left side (SPS's upper punch), while the grain size on the right side (SPS's lower punch) is uniform. Both images were taken in the BSE mode. In the case of the **(b)**, the black areas are contamination from the graphite felt caused during the SEM observations as both sides of the fracture were examined.

Fig. 3. Details of fracture by FSPS of HfB_2 monoliths: (a)–(c) show fracture surfaces of HfB_2 after the FSPS following flexural test at room temperature, while (d)–(f) are after the flexural strength test at 1600 °C. Note the chaotic distribution of the large grains in (a) and (d) does not change. (g) shows typical loading diagrams observed flexural strength test for bars in (c),(f). High-temperature data at 600 °C and 1200 °C were collected using a single test and

are presented in order to show the tendency in the flexural strength behavior at elevated temperatures.

Fig. 4. SEM images of HfB_2 ceramic obtained by CSPS (2000 °C/ 5 min) after flexural test at (a,c) room temperature and (b,d) 1600 °C. Mind that for (a) and (b), the majority of pores are located within the grains, and have both spherical and elongated shapes; (b) shows that some of the grains were fractured in a trans-granular manner. (e) compares the data of HfB_2 obtained in this study with previously obtained results for HfB_2 [2,3,6,18] and TaB_2 [19]. In the case of the bimodal structure for the FSPS the data points correspond to the large and fine grains.

Fig. 5. Temperature dependence of shrinkage for the powder specimen during FSPS experiments using a Sumitomo unit (#66 F). One can see three distinctive zones: (1) pyrometer adjustment, (2) flash sintering and (3) a zone for a short dwell. The displacement rate is provided as the red dashed line.

Fig. 6. Shrinkage rate for the powder specimen during the FSPS experiments using a Sumitomo unit (#66F) as a function of the inverse temperature. The temperature was experimentally determined (see section 3.1). One can see that roughly the same three zones can be noticed. The Figure (b) inset shows the elevated temperature dependence of the shrinkage in detail. Mind the presence of the area where the temperature decreased after reaching 2000 °C. At this point, the temperature was manually controlled using the current value, and after a short dwell during which the temperature rapidly increased, the SPS unit was turned off.

Fig. 7. Shrinkage rate for the powder specimen during the FSPS experiments using a Sumitomo unit (#66F) as a function of the inverse temperature. One can see that roughly the same three zones can be observed. Importantly, a linear behavior of the densification rate between 860 °C and 1760 °C allows estimation of the activation energy.

Fig. 8. Evaluation of the activation energy for the hafnium diboride consolidated by flash spark plasma sintering. Additional data points show the effect of the possible error associated with the temperature measurement. The evaluated values of the apparent activation energies were evaluated by linear fitting.

Fig. 9. Schematic diagrams showing contribution of main processes at consolidation on different stages of the process. Temperature zone for the flash processes (FSPS) is indicated. Note that because grain growth in a porous body requires a higher temperatures, development of bimodal structures is expected if the bulk overheating and hot-spot generation are active. (b) shows that in the case of the grain growth accelerated at higher temperatures requires a lower driving force, and has a higher growth rate. These two factors allow one to obtain ceramics with a bimodal grain size (possible window of opportunity). Heating rate underline finding of [35] for alumina, where surface diffusion was avoided while using heating rate of 600 °C/min.

Fig. 10. Details of fracture of FSPSed of HfB_2 monoliths at ambient temperature: (a) and (b) show macroscopic images of flexure bars after the tests, while (c) present loading curves observed during fracture. Large-sized grains with identical grain size were highlighted in (a) and (b) in order to show their distribution.

Fig. 11. Effect of temperature on the flexural strength of transition metal diborides [2,25,38–40] and diboride–diboride composite [41]. Argon was used during the high-temperature flexural test for all the reported data. The dashed line for the ZrB_2 ceramics indicates the general tendencies observed in previous studies [38,39]. The closed symbols indicate that the strength was measured using a four-point setup and the open symbols show the results of the three-point flexural strength tests.

Tables

Table 1 Experimentally determined activation energy, and estimated sintering mechanism for transition metal diborides of the IV group.

Diboride	Consolidation method	Applied pressure, MPa	Activation energy, kJ/mol	Possible mass transport mechanism
HfB_2	FSPS	20	99	Volume diffusion*
			66	Grain-boundary diffusion*
HfB_2	FSPS error of +100 °C is assumed	20	74	Volume diffusion*
			111	Grain-boundary diffusion*
HfB_2	FSPS error of +300 °C is assumed	20	90	Volume diffusion*
			132	Grain-boundary diffusion*
HfB_2 [28]	High-pressure hot-pressing	790	96	Volume diffusion of boron, or stress-directed grain boundary diffusion of hafnium
ZrB_2 [29]	Hot-pressing	50	695±62	Volume diffusion
ZrB_2 [30]	Pressulress sintering	-	416±174 and 678±114	-
TiB_2 [31]	Pressureless sintering	-	774±46	Volume diffusion
TiB_2 [32]	Microwave sintering	-	850±60 and 638±20	-
Boron diffusion in TiB_2 [33]		-	190	Volume diffusion

* It is assumed that this is volume of grain boundary diffusion of B in HfB_2, based on findings in [28] and [33]. Metal atoms usually have an activation energy of bulk diffusion in diboride lattice ~ 1000 kJ/mol, see for instance [19].

Figure 1

Click here to download high resolution image

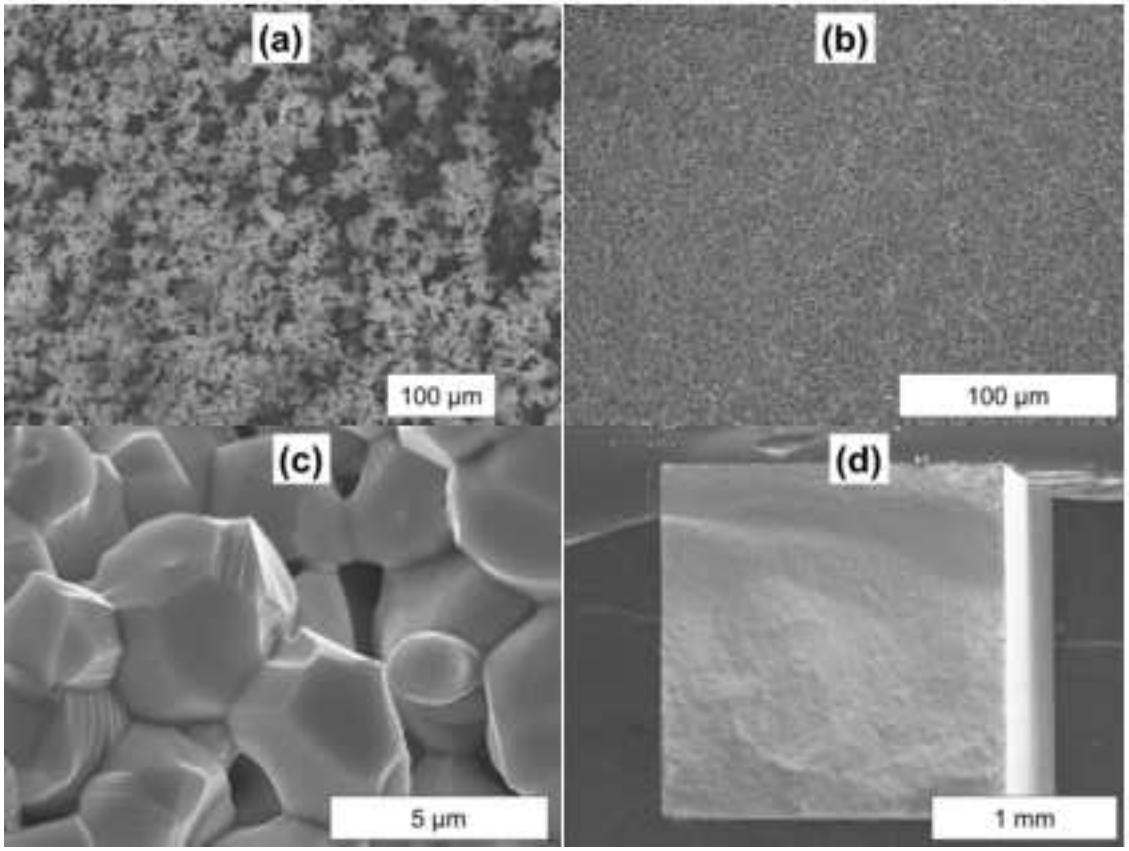

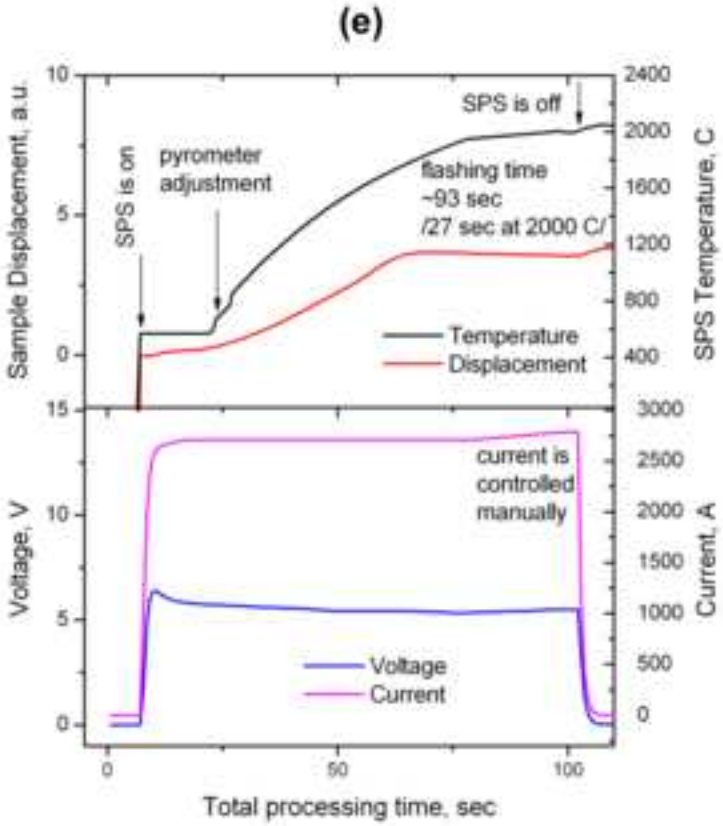

Figure 2

Click here to download high resolution image

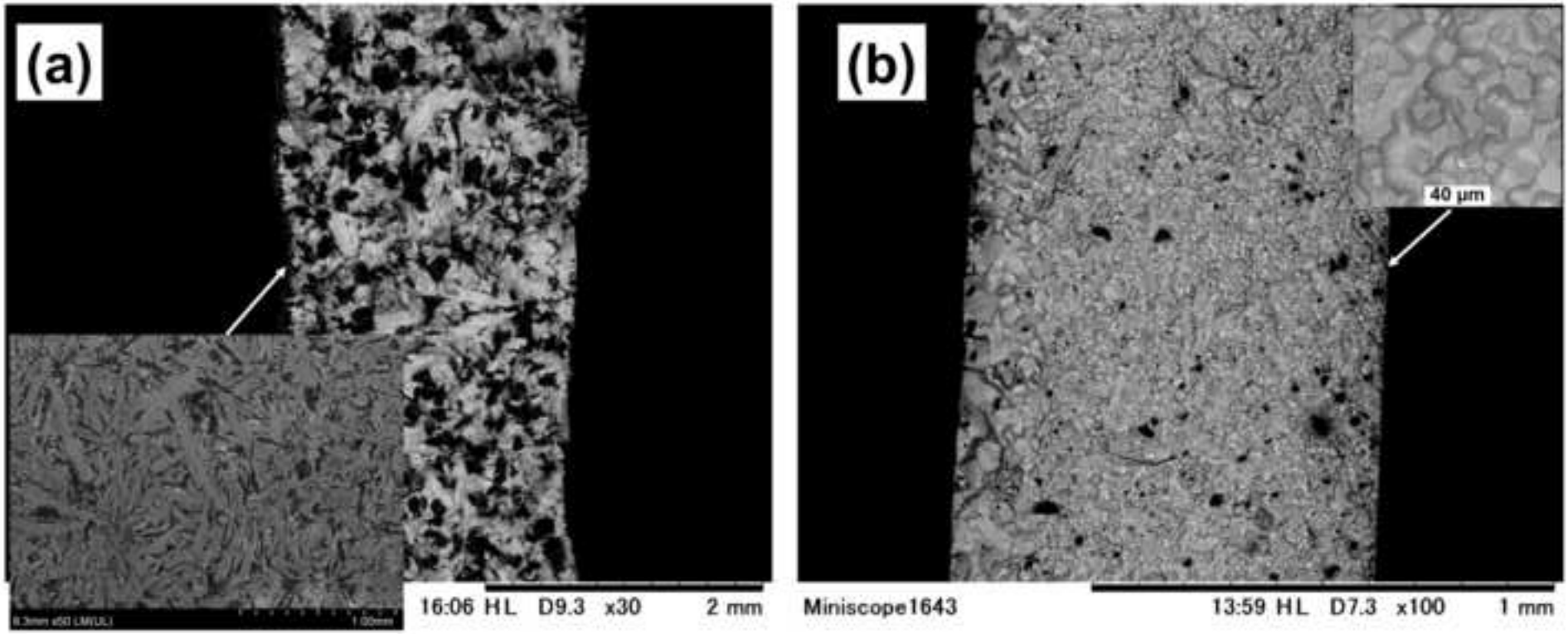

Figure 3

Click here to download high resolution image

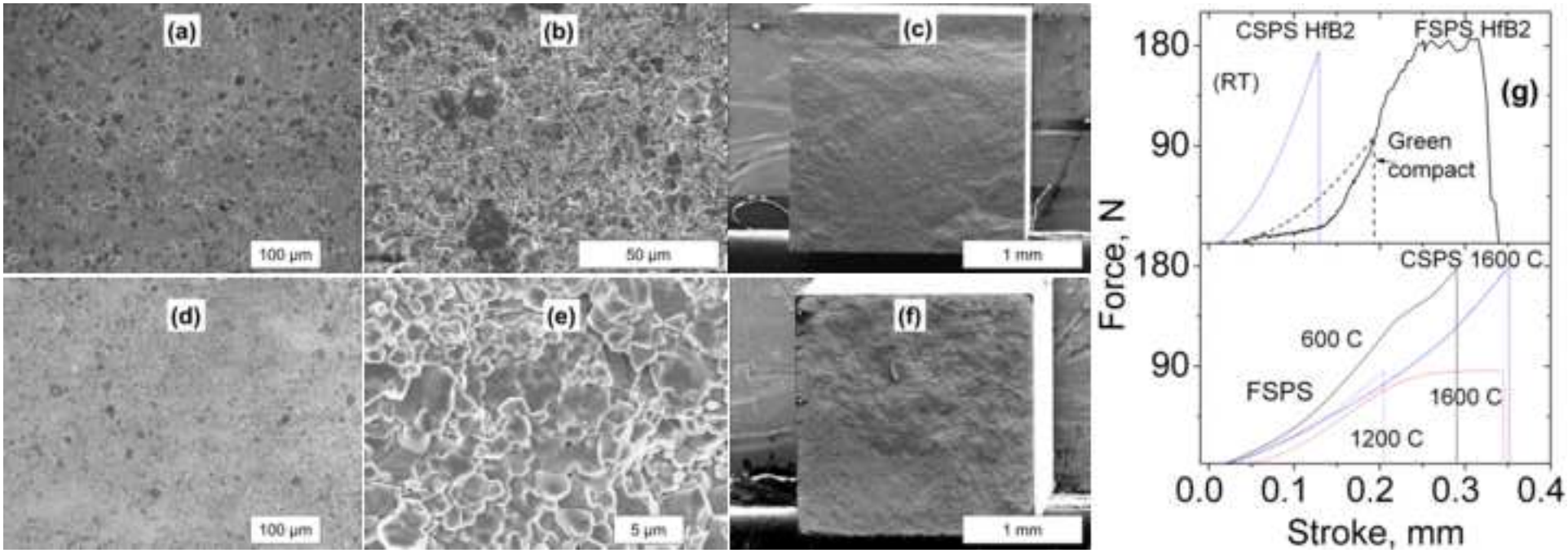

Figure 4

Click here to download high resolution image

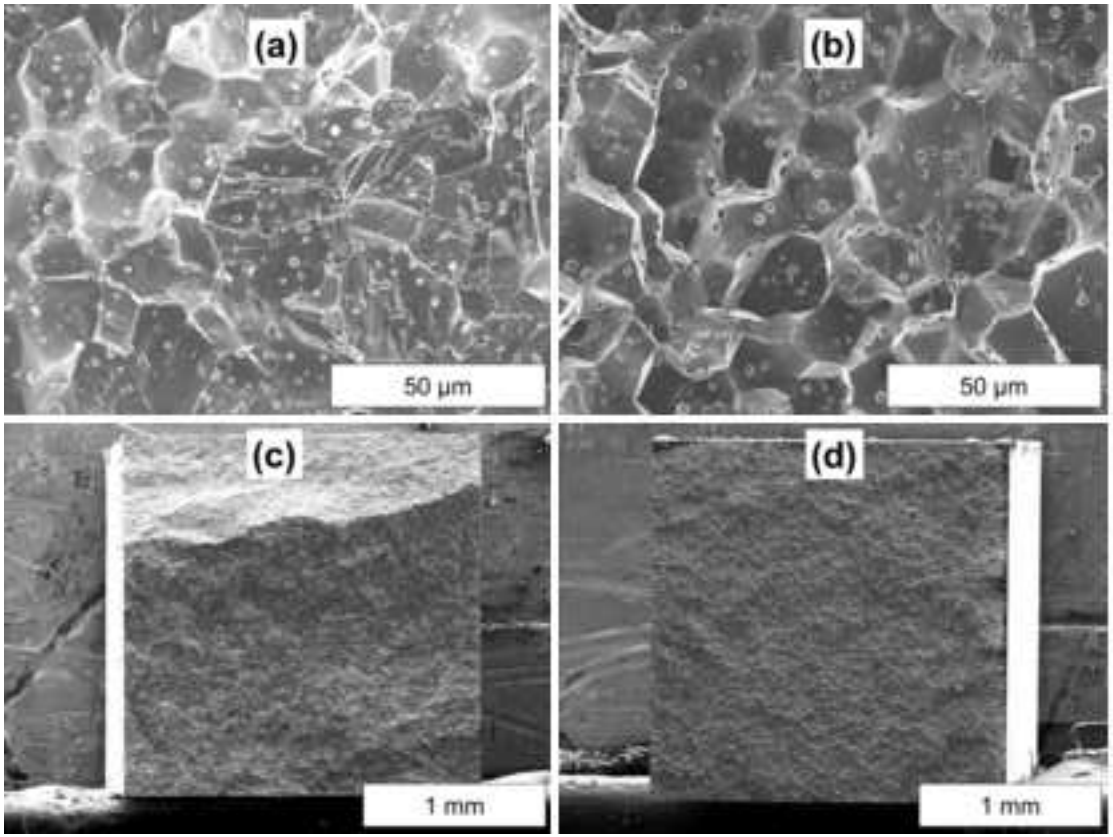

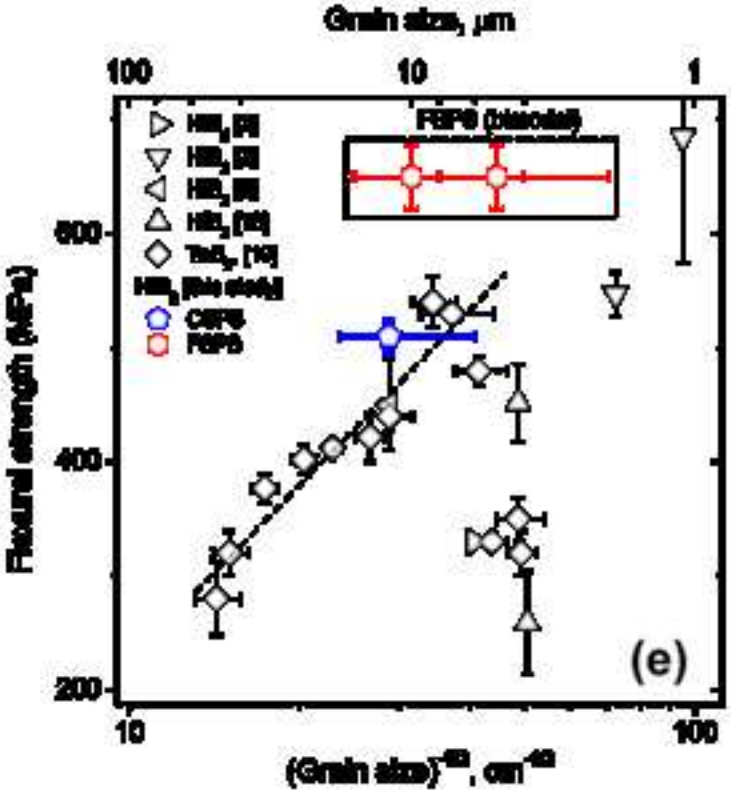

Figure 5

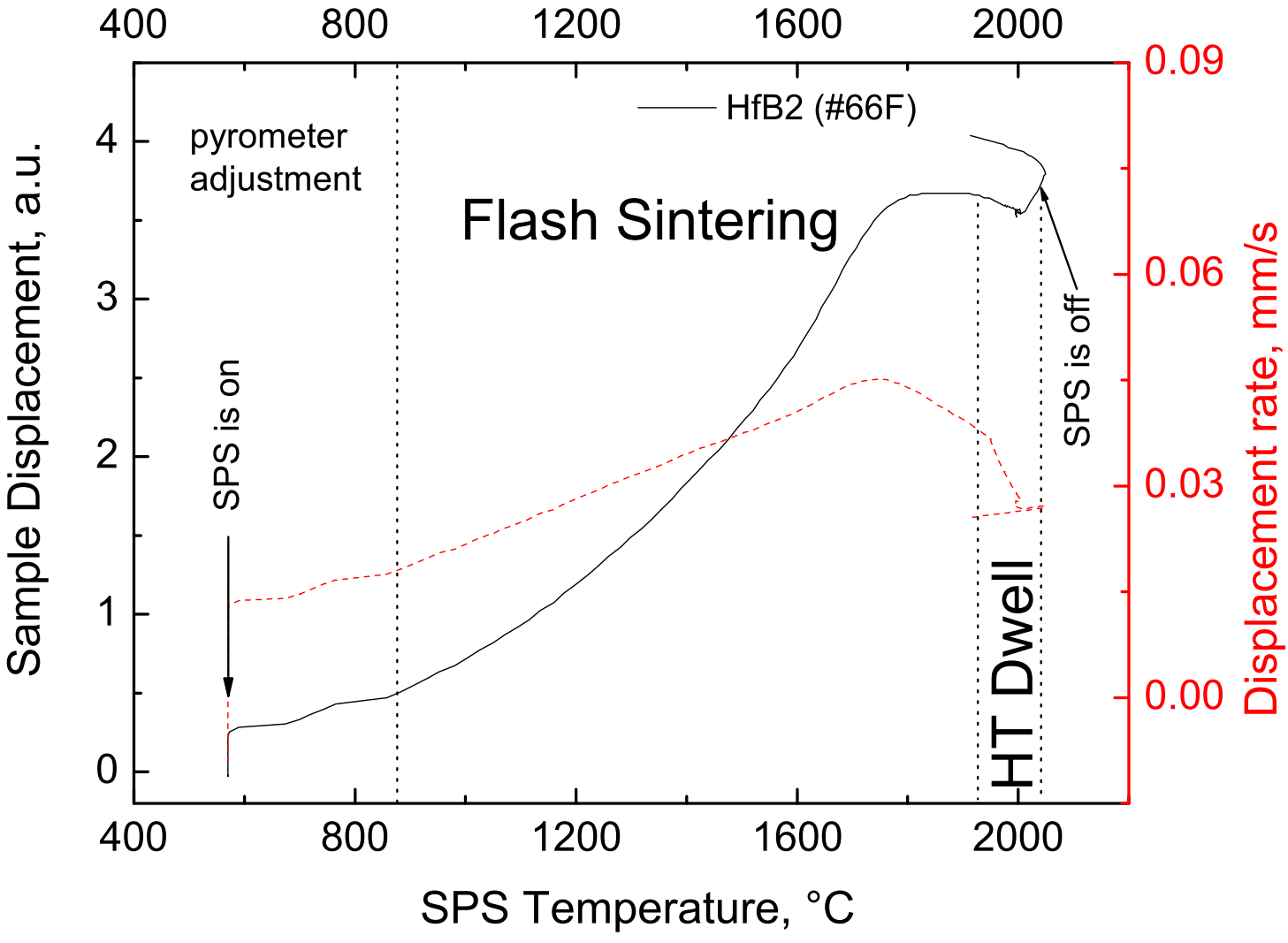
400
800
1200
1600
2000
0.09
0.06
0.03
0.00
HfB2 (#66F)
pyrometer
adjustment
Flash Sintering
SPS is on
SPS is off
HT Dwell
Sample Displacement, a.u.
Displacement rate, mm/s
SPS Temperature, °C
0
1
2
3
4

Figure 6

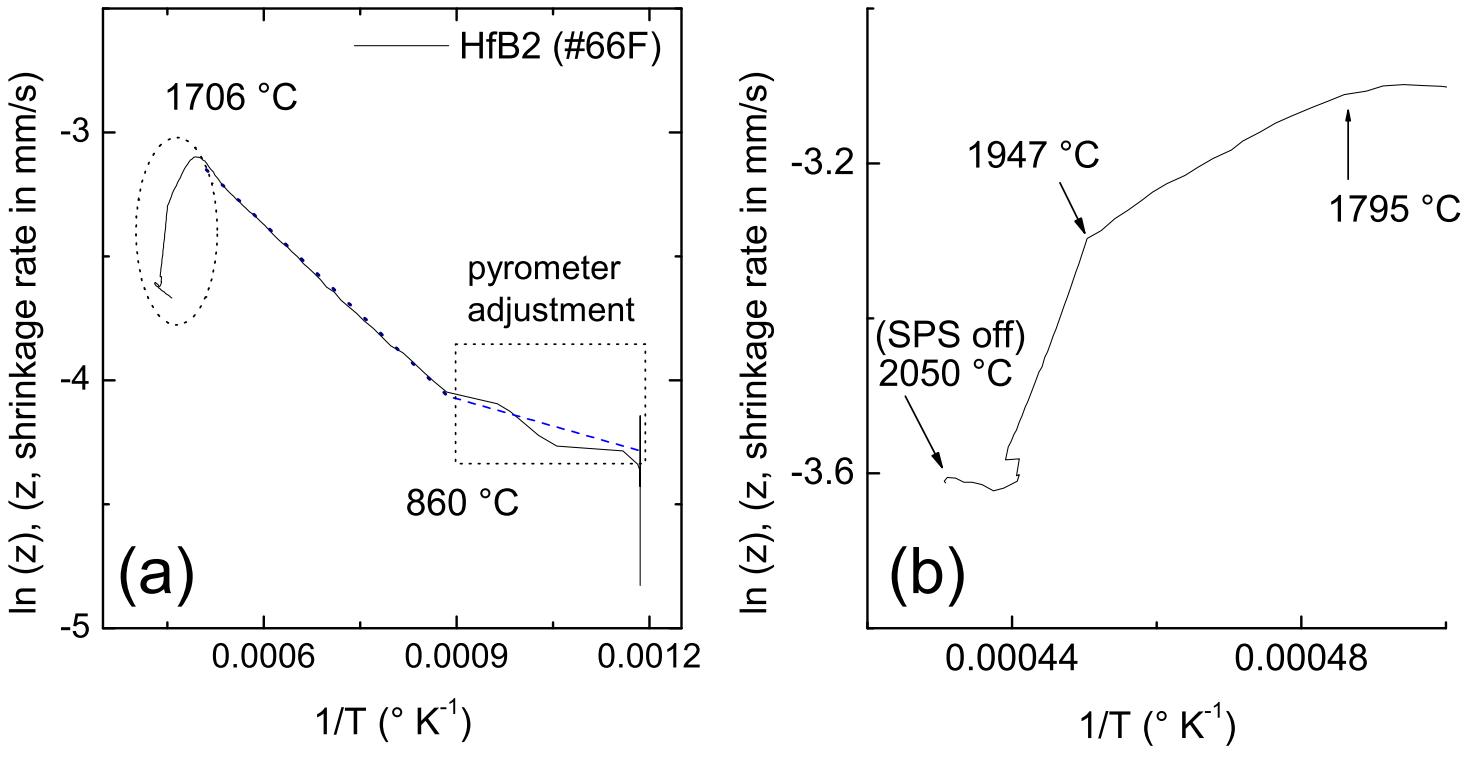
HfB2 (#66F)
1706 °C
pyrometer
adjustment
860 °C
(a)
ln (z), (z, shrinkage rate in mm/s)
-3
-4
-5
0.0006
0.0009
0.0012
1/T (° K-1)
1947 °C
1795 °C
(SPS off)
2050 °C
(b)
-3.2
-3.6
0.00044
0.00048

Figure 7

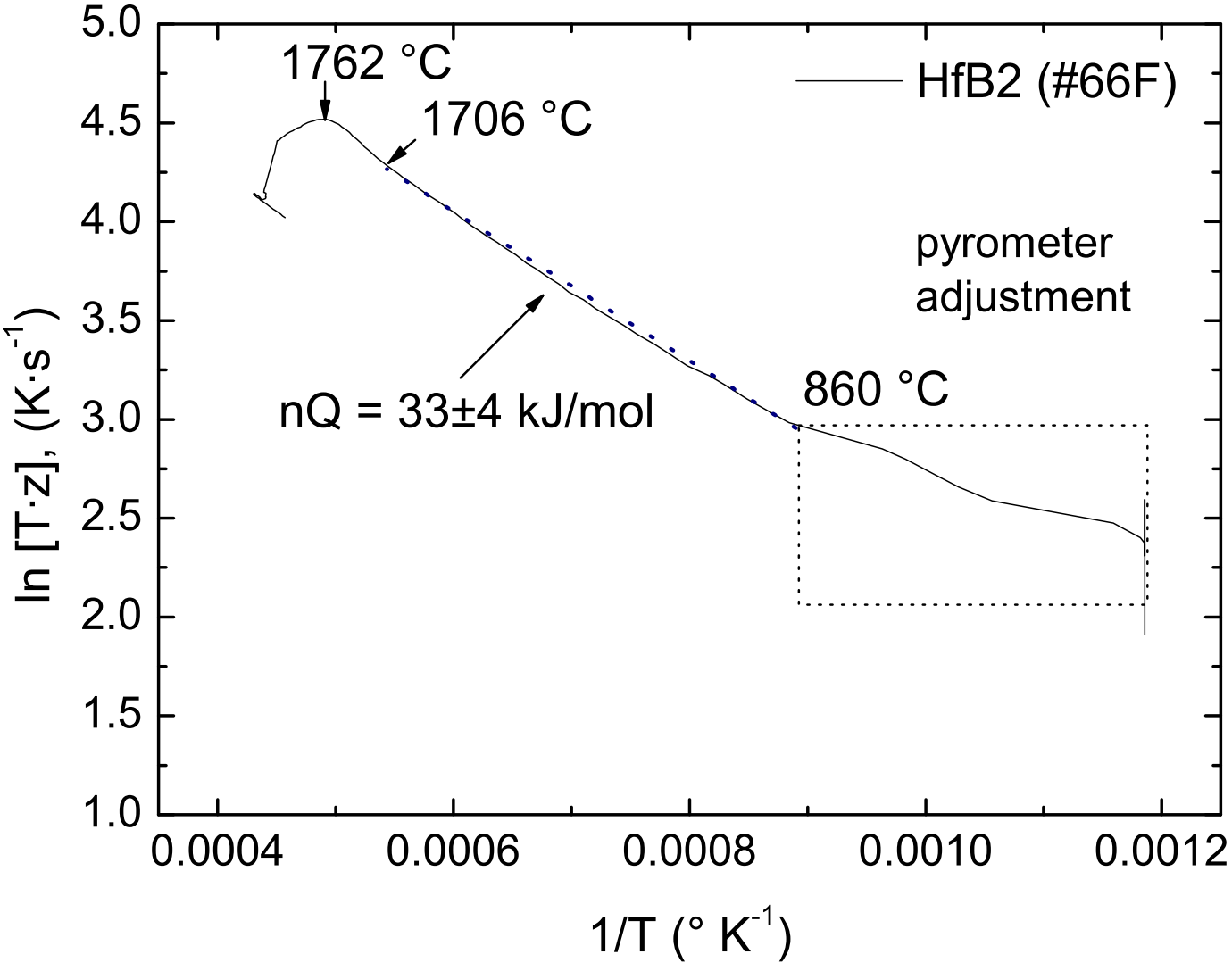
1762 °C
1706 °C
HfB2 (#66F)
pyrometer
adjustment
nQ = 33±4 kJ/mol
860 °C
ln [T·z], (K·s-1)
1/T (° K-1)
5.0
4.5
4.0
3.5
3.0
2.5
2.0
1.5
1.0
0.0004
0.0006
0.0008
0.0010
0.0012

Figure 8

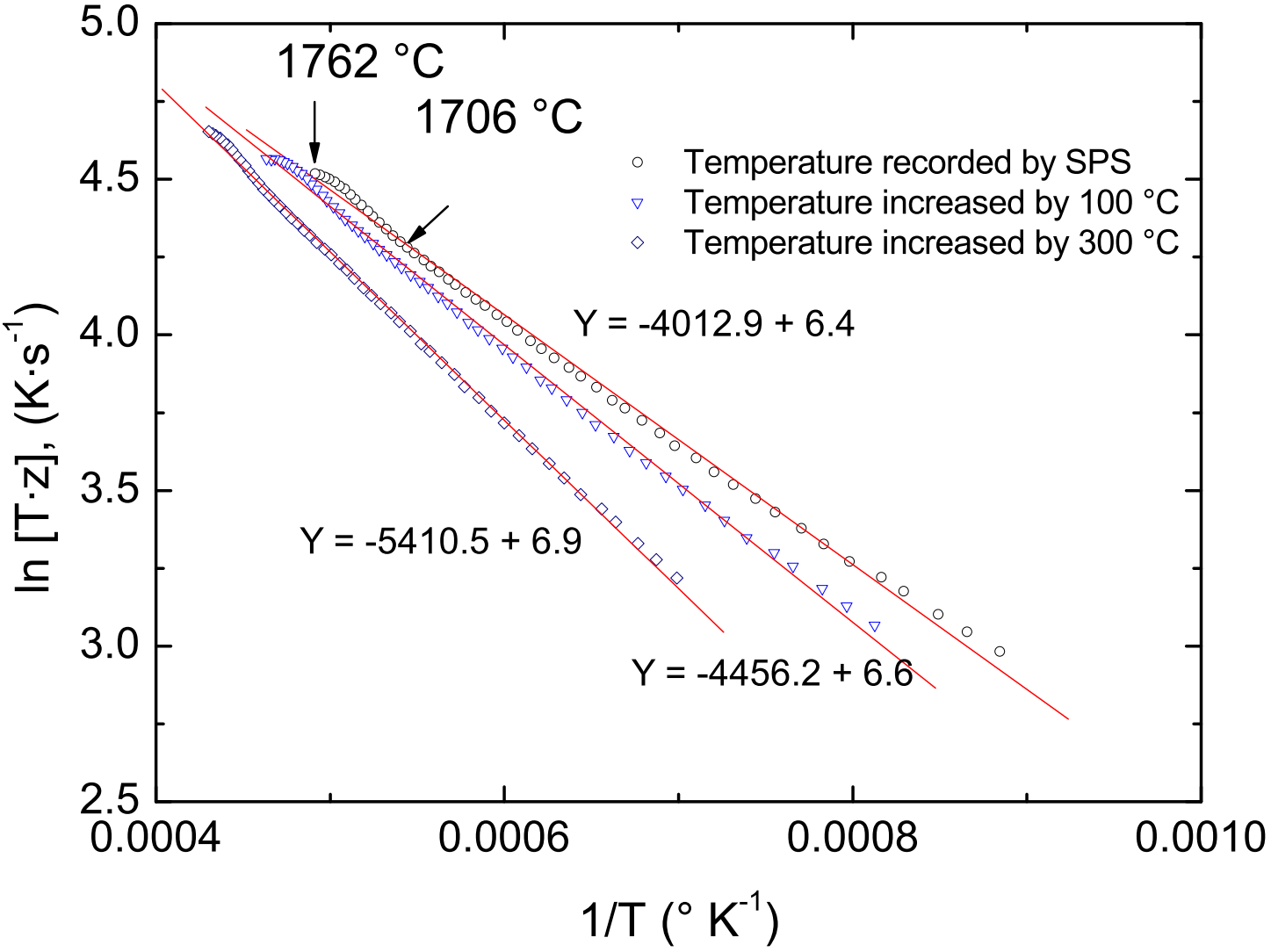
5.0
4.5
4.0
3.5
3.0
2.5
0.0004
0.0006
0.0008
0.0010
ln [T·z], (K·s-1)
1/T (° K-1)
1762 °C
1706 °C
Temperature recorded by SPS
Temperature increased by 100 °C
Temperature increased by 300 °C
Y = -4012.9 + 6.4
Y = -5410.5 + 6.9
Y = -4456.2 + 6.6

Figure 9

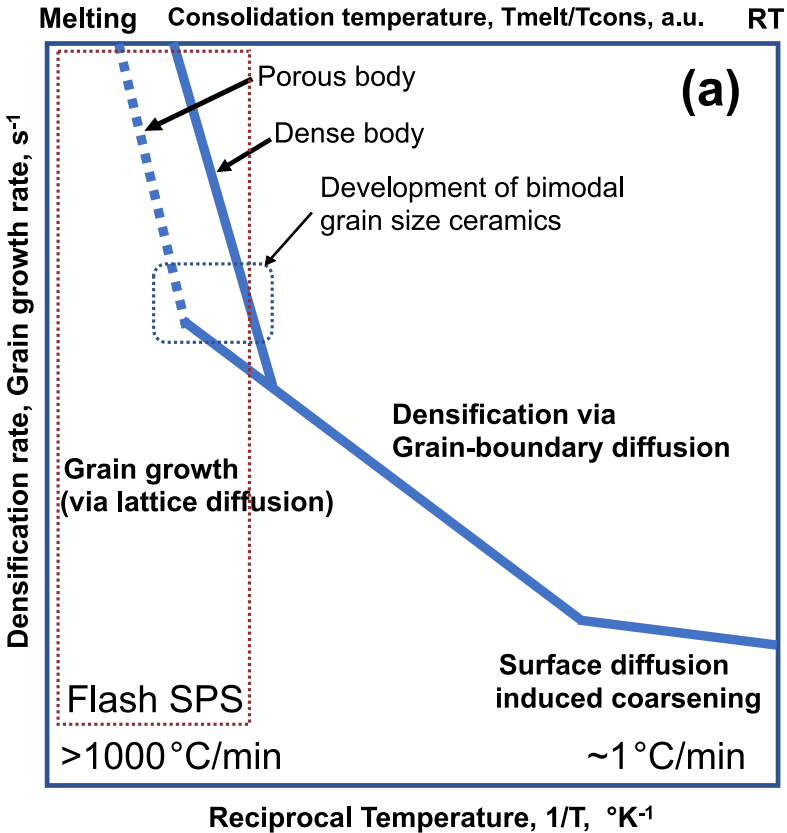
Melting
Consolidation temperature, Tmelt/Tcons, a.u.
RT
Porous body
Dense body
Development of bimodal grain size ceramics
(a)
Densification via Grain-boundary diffusion
Grain growth (via lattice diffusion)
Surface diffusion induced coarsening
Flash SPS
>1000 °C/min
~1 °C/min
Densification rate, Grain growth rate, s-1
Reciprocal Temperature, 1/T, °K-1

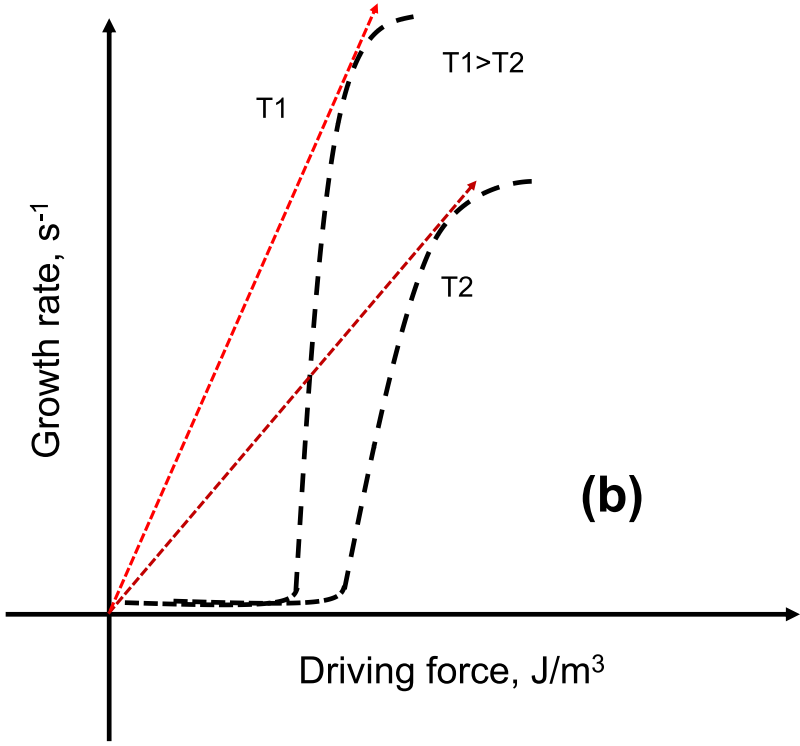
T1
T1>T2
T2
(b)
Growth rate, s-1
Driving force, J/m3

Figure 10

Click here to download high resolution image

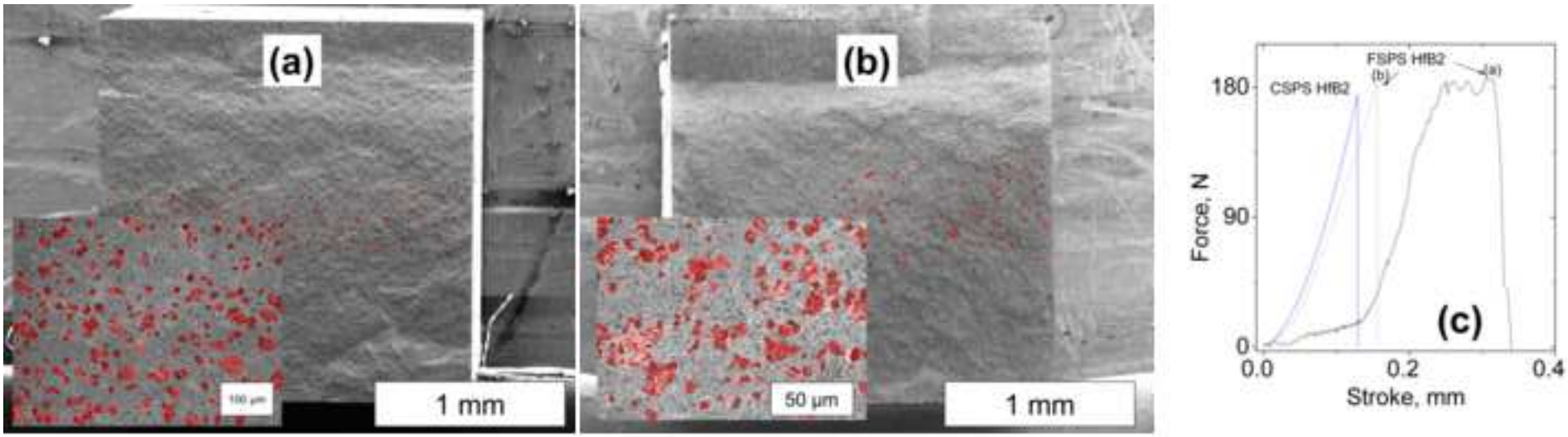

Figure 11

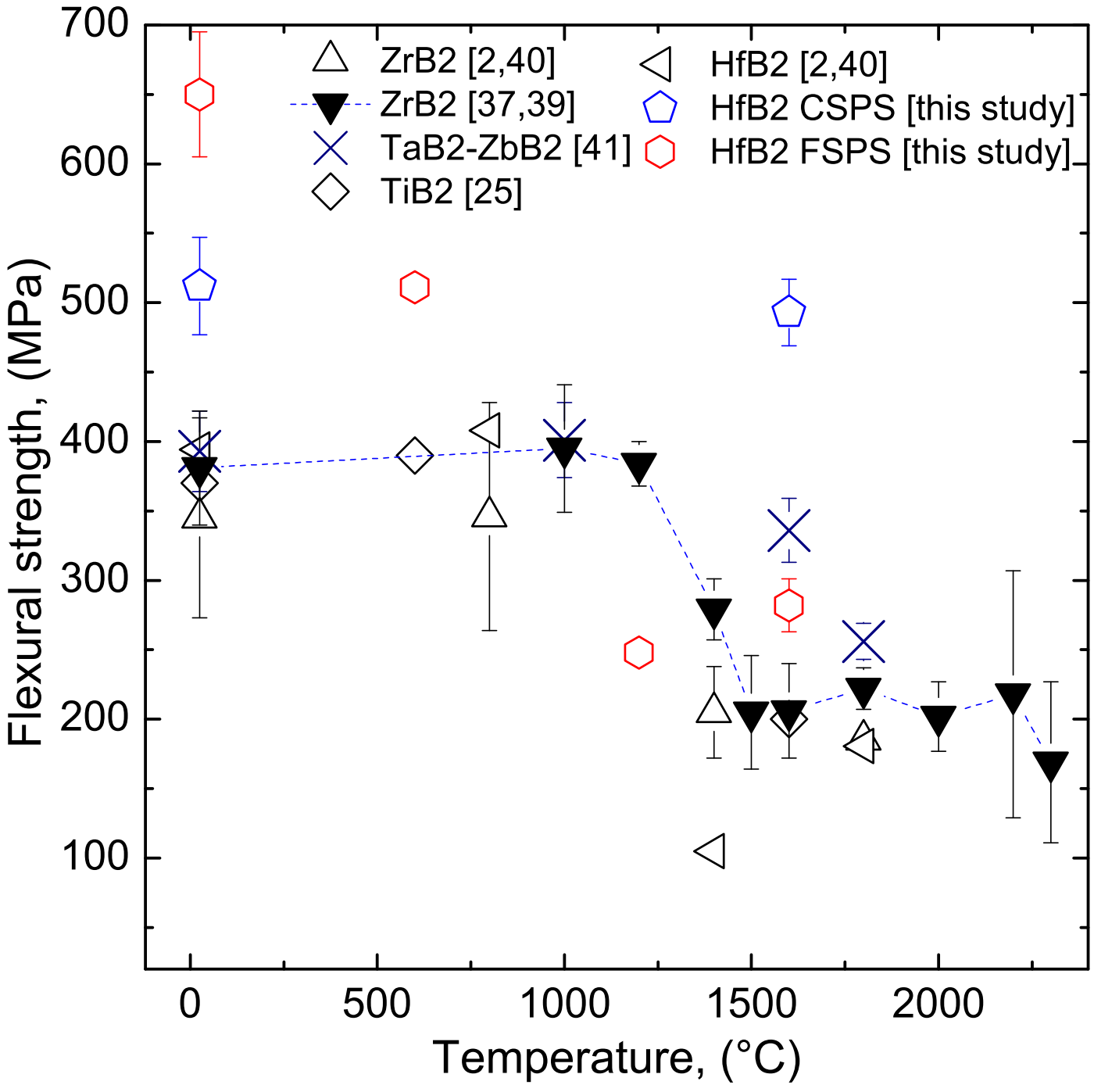
ZrB2 [2,40]
ZrB2 [37,39]
TaB2-ZbB2 [41]
TiB2 [25]
HfB2 [2,40]
HfB2 CSPS [this study]
HfB2 FSPS [this study]
Flexural strength, (MPa)
Temperature, (°C)
700
600
500
400
300
200
100
0
500
1000
1500
2000